Check for updates

Directional mass transfer of azo molecular glass microsphere induced by polarized light in aqueous immersion media†

Hao Huang, [ID] [a] Zenan Wang,[a] Xu Li,[a] Fan Yang,[b] Yechao Su,[c] Jianhong Xu [ID] [c] and Xiaogong Wang [ID] *[a]

Photoinduced mass transfer of azo polymer and azo molecular glass has been intensively investigated under various light irradiation conditions simply using air as the ambient environment. In this work, in order to understand the effects of the surrounding medium on the light-induced process, azo molecular glass microspheres adhered on a substrate were immersed in water and different aqueous solutions, and their mass transfer behavior was investigated by irradiation with linearly polarized light. The microspheres in the aqueous media showed significant deformation through directional mass transfer upon light irradiation and transformed into a series of shape-anisotropic particles as revealed by microscopic observations. Compared with their counterparts upon light irradiation in air, the particles immersed in the aqueous media exhibited larger elongation parallel to the substrate and higher shape anisotropy. Optical simulation showed that this was caused by the alteration of the direction of the electric vibration of the refracted light at the medium–microsphere interface, which controlled the mass transfer behavior. On the other hand, the viscosity of the aqueous media showed no effect on the mass transfer process induced by the irradiation. The photo-thermal effect on the mass transfer behavior was ruled out as the thermal dissipation through a liquid is much more efficient than that through air. On the basis of this, this methodology was also successfully employed in the photo-fabrication of anisotropic submicron-sized periodic structures in aqueous medium. These observations can supply deep understanding of this fascinating process induced by polarized light and extend the scope of its applications.

Introduction

Photoinduced mass transfer is an intriguing function of azochromophore-containing soft matter (*i.e.* azo polymer and azo molecular glass), which has been intensively investigated for understanding its mechanism and extending its applications in different areas.[1–9] Previous studies show that upon light irradiation at an appropriate wavelength, the repeated *trans–cis* photoisomerization cycles of azo chromophores at the molecular level can drive the macroscopic mass migration of the materials.[1–6] This effect was first observed for the surface-relief-grating (SRG) formation on the azo polymer films upon exposure to the interference fringes formed by two coherent laser beams.[10,11] This type of mass transfer is highly directional and preferentially occurs along the electric

[a]Department of Chemical Engineering, Laboratory of Advanced Materials (MOE), Tsinghua University, Beijing 100084, People's Republic of China. E-mail: wxg-dce@mail.tsinghua.edu.cn

[b]Department of Physics, State Key Laboratory of Low Dimensional Quantum Physics, Tsinghua University, Beijing 100084, People's Republic of China

[c]Department of Chemical Engineering, The State Key Lab of Chemical Engineering, Tsinghua University, Beijing 100084, People's Republic of China

† Electronic supplementary information (ESI) available. See DOI: 10.1039/d1ra01904j

vibration direction of the polarized light.[12–16] The underlying mechanism of the directional mass transfer has been actively investigated from different aspects.[17–27] Meanwhile, its application has been demonstrated to implement the morphology and shape manipulations of solid films and nano/microstructures, which include surface patterning,[8,16,28–30] optical near-field mapping,[3,31,32] biomolecule immobilization,[33] cell-guiding substrates,[7,34–36] and others. With all these progresses, understanding its mysterious nature and broadening the platform for other applications are still in the research frontier at the current stage.

Distinct from SRG formation induced by two interfering laser beams, photoinduced deformation of microspheres of azo polymer and azo molecular glass is actuated by a single beam or uniform light field.[15,37–44] By irradiation with linearly polarized light, the directional mass transfer can cause significant elongation of the microspheres along the electric vibration direction of the electromagnetic wave.[37,38] Through this approach, shape-anisotropic particles with diversified morphologies (*e.g.*, ellipsoidal, rod-like, mushroom-like and acorn-like ones) can be controllably fabricated from the microspheres, and their three-dimensional (3D) shapes can be dynamically manipulated in a non-touched manner.[39–45] This shape manipulation approach can be applied in some appealing fields such as surface wettability

modification,[39] photo-alignment of inorganic nanoparticles,[42,43] and anisotropic light diffusers.[45] The photoinduced deformations of azo polymer microspheres have been found to correlate with the excitation wavelength,[38] the microsphere size,[42–44] and the azo chromophore content.[44] Azo molecular glass, a type of low-molecular-weight amorphous organic material containing azo chromophores, has recently been used as an ideal substance for studying this type of light-induced behavior.[39,40] The well-defined chemical structure and the absence of chain entanglements of polymers not only endow the azo molecular glass with sensitive response to the light irradiation, but also simplify the analysis of the correlation with structural factors.[46–48] For this reason, the microspheres and particles made of azo molecular glass have been investigated to elucidate the effects of light wavelength,[39] particle size,[39] and light polarization state.[40]

In most of the previous reports, the photoinduced mass transfer and deformations of the microspheres, made of both azo polymers and azo molecular glasses, have been investigated under the air-ambient condition,[15,37–45] few in gels,[49] and in elastomers.[45,50] In the light irradiation process, using a medium instead of air will alter the light refraction condition at the interface. As the mass transfer occurs along the direction of the electric vibration of the polarized light, the immersion medium (or surrounding environment) could have important effects on the results. Also, the medium will modify the transport environment around the microspheres, such as heat dissipation and diffusion, which could also show some influences. Nevertheless, for a medium like gel or elastomer, the mechanical strength of the medium is dominant over other factors such as refractive index and thermal conductivity to show their effects. Water as a good immersion medium has been typically used in photo-lithography to enhance the resolution of nano-fabrication,[51] and in interferometric lithography to reduce the minimum half-pitch.[52] For light-responsive particles, the shape-adaptability/reconfigurability in aqueous environment show remarkable significance for various biological technologies such as drug delivery and vascular transportation.[53,54] The study of the photoinduced mass transfer of microspheres in aqueous immersion media will be of benefit to understanding the intricate nature of the photoinduced mass transfer of azo polymers and azo molecular glasses, and possible to offer an efficient methodology for manipulating the soft-matter architectures for many future applications. A preliminary experiment about the photoinduced deformation of azo polymer colloidal spheres trapped at water/glass interface has been briefly reported in a recent article by Loebner et al.[50] However, the direct comparison of particle deformations in air and in water was not accomplished in the work since the irradiation wavelength differs for both experiments (491 and 355 nm, respectively). To our knowledge, a systematic study of the photoinduced mass transfer behavior of the azo-chromophore-containing microspheres in aqueous immersion media to fully understand their influences has not been reported in the literature yet.

In this study, we investigated the photoinduced deformation of a type of azo molecular glass (IAC-4) microspheres in water and aqueous solutions to elucidate the unique effect of the immersion medium on the mass transfer behavior. For this purpose, IAC-4 microspheres with the monodispersed diameter around 14.7 μm were fabricated and adhered on the silicon substrate. When immersed in water and a series of aqueous solutions with different refractive indices and viscosities, the microspheres were subjected to the irradiation of the linearly polarized light at 488 nm. The shape deformations as a result of the mass transfer were examined by microscopy on the obtained particles. It was observed with interest that the mass transfer could be induced in the aqueous media with high efficiency, through which the IAC-4 microspheres were transformed into shape-anisotropic particles in a well-controlled manner. The three-dimensional (3D) morphology and surface flatness of the obtained particles were thoroughly characterized by the microscopic observations. The refractive index was proved as the dominant factor to control the photoinduced mass transfer and shape deformation in different media. The related mechanism was elucidated through the optical calculation by considering the light refraction and electric field energy distribution at the liquid–microsphere interface. On the other hand, the viscosity of the immersion medium showed negligible influence on the shape evolution process. To step from the understanding to a feasible methodology, the photoinduced deformation was also tested using the submicron-sized periodic structures of IAC-4. The patterns with the large shape-anisotropy were obtained in the water immersion medium, compared with those obtained in the air-ambient environment under the same irradiation condition.

Experimental

Materials

The azo molecular glass (IAC-4, Chart 1) was synthesized according to the previous report.[48] The characterization results of IAC-4 are shown in Fig. S1–S4 (in ESI†). Monodispersed IAC-4 microspheres with the averaged diameter of 14.7 ± 0.1 μm were fabricated via the emulsion-solvent evaporation method in a microfluidic chip.[40] Potassium thiocyanate (KSCN, 99%) was purchased from Sigma-Aldrich. Poly(vinyl alcohol) (PVA) with the hydrolysis degree of 98–99% and the averaged molecular weight of 88 000–97 000 was purchased from Alfa Aesar. Deionized water (resistivity > 18 MΩ cm) was obtained from a Milli-Q water purification system. Other reagents and solvents were purchased from commercial sources and used as received without further purification.

Preparation of aqueous solutions

The aqueous solutions of KSCN with different concentrations (30 wt%, 52 wt% and 70 wt%) were prepared at the temperature
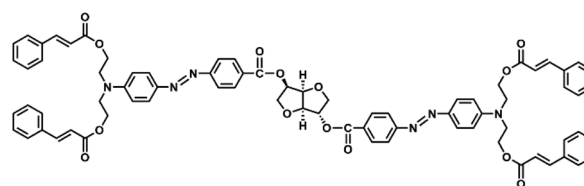

Chart 1 Chemical structure of the azo molecular glass IAC-4.

of 25 °C under sonication, which were then filtered through 0.45 µm syringe membranes to remove the particulate impurities. The aqueous solutions of PVA with different concentrations (2.5 wt%, 5 wt% and 8 wt%) were prepared at the temperature of 90 °C under mechanical stirring for 12 h. After cooled down to room temperature, the viscous PVA solutions were filtered under reduced pressure to remove the particulate impurities. The as-prepared solutions were all colorless and transparent liquids, which could be stably stored in the sealed glass bottles at the constant temperature (25 °C) for months. The physical properties and image of the aqueous solutions are given in Table S1 and Fig. S5 (in ESI†).

Immobilizing IAC-4 microspheres on substrate

Poly(butyl acrylate) (PBA), a soft and sticky polymer at room temperature, was served as an adhering layer to immobilize the IAC-4 microspheres on the silicon substrate. The synthesis and characterization of PBA are shown in ESI.† Before loaded with the microspheres, a piece of the clean silicon wafer (in a rectangular shape of *ca.* 10 mm × 8 mm) was spin-coated with the CHCl$_3$ solution of PBA (2 wt%) at the spinning speed of 1000 rpm, which was then dried in a vacuum oven at 30 °C for 48 h. The thin film of PBA with smooth surface was formed and the thickness of the film was about 900 nm. Then, a few drops of water suspension containing IAC-4 microspheres were casted onto the PBA-coated substrate. After left aside for several minutes, the redundant liquid was gently removed from the sample surface. This procedure ensured that the IAC-4 microspheres were tightly adhered by the PBA layer and dispersed on the substrate as isolated particles.

Light irradiation on IAC-4 microspheres in aqueous medium

Photoinduced mass transfer of IAC-4 microspheres was investigated by irradiation in an aqueous medium, where the composition and concentration were purposefully predesigned. In the process, a piece of the silicon substrate loaded with IAC-4 microspheres was immersed in the aqueous medium in an open Petri dish. The height of liquid above the sample surface was controlled to be about 8 mm for each case. A linearly polarized laser beam (λ = 488 nm, Genesis CX 488-2000 SLM, Coherent Corporation) was expanded with a spatial filter and collimated by a plano-convex lens to generate a homogeneous beam with the spot size of 20 mm in the diameter. Then, the laser beam was reflected by a 45° mirror to illuminate the sample in the aqueous medium at normal incidence. The light intensity on top of the aqueous medium (*i.e.*, after the 45° mirror) was controlled to be 200 mW cm^{-2} for each case. To benefit the morphological characterization in the following investigation, the long side of silicon substrate was parallel to the electric vibration direction of the incident light (*i.e.*, the long axis of the elongated particles). After being irradiated for a period of time, the sample was gently lifted out of the aqueous medium, rinsed with deionized water, and dried in ambient conditions. For the control experiment where air served as the surrounding medium, the sample was placed in a Petri dish

without the immersion liquid and the other parts of the procedure were the same.

Instrument and characterization

Light transmittance spectra of the aqueous media were obtained using an Agilent 8453 UV-vis spectrophotometer in a quartz cuvette with the optical path of 1 cm. The refractive index of aqueous medium (n_{me}) at the Fraunhofer D-line (λ = 589.3 nm) was measured by an Abbe refractometer (WAY-2W, Shanghai Shenguang Instrument Co., Ltd). Concerning the optical dispersions of these liquids are negligible in the visible range (Table S1 in ESI†), the measured n_{me} can be regarded as the refractive index at the laser wavelength (λ = 488 nm). The viscosity of aqueous medium (η_{me}) was measured by an Ubbelohde viscometer at the temperature of 30 °C. The inner diameter of the capillary was 1.07 mm. Before measurements, the viscometer was calibrated using several standard liquids with known viscosities, and the details can be seen in ESI (Fig. S6†). The glass transition temperature (T_g) of IAC-4 was measured by differential scanning calorimetry (TA instruments DSC 2920) with a heating rate of 10 °C min^{-1} in nitrogen atmosphere. The refractive index (n_{azo}) and extinction coefficient (κ_{azo}) of IAC-4 were measured by an ellipsometer (SE850, Sentech Instruments) at the incident angle of 70°. The film samples for the ellipsometry were prepared by spin-coating the CHCl$_3$ solution of IAC-4 (3 wt%) onto the silicon wafer and vacuum drying at 45 °C for 24 h. Nanoindentation tests were performed on the Nano Indenter G200 (Keysight) system using a Berkovich-type diamond indenter tip. The maximum indentation depth was 1000 nm with the loading rate of 10 nm s^{-1}. The film samples for the nanoindentation tests were prepared by dip-coating the DMF solution (5 wt%) of IAC-4 onto clean glass slides, evaporating solvents at 80 °C and drying at a vacuum oven. The morphologies of the IAC-4 microspheres and deformed particles were obtained using a Gemini300 (Zeiss Corporation) scanning electron microscope and observed from two orthogonal views (front-view and top-view). The accelerating voltage and the aperture size were 5 kV and 60 µm, respectively. Before SEM observations, the samples were sputtered with a thin layer of gold with the thickness of about ten nanometers to enhance the conductivity. To acquire the front-view SEM images, the samples were vertically adhered onto the upright wall of a cross-sectional stage, and the long side of silicon substrate (*i.e.*, the elongation axis of deformed particles) was orientated in the horizontal direction. The optical microscopic (OM) images of the IAC-4 microspheres and deformed particles were obtained on a Nikon LV 100POL microscope in the reflection mode and captured by a Nikon DS-fi2 CCD camera. The objective lens with the numerical aperture (NA) of 0.55 and magnification of 50× was used.

Results and discussion

The monodispersed azo molecular glass (IAC-4) microspheres with the diameters of 14.7 ± 0.1 µm were used for the investigation. Compared with the azo microspheres with smaller and larger sizes (sub-micron and hundred-micron),[37,44] these ten-micron-sized IAC-4 microspheres exhibit the richness of the
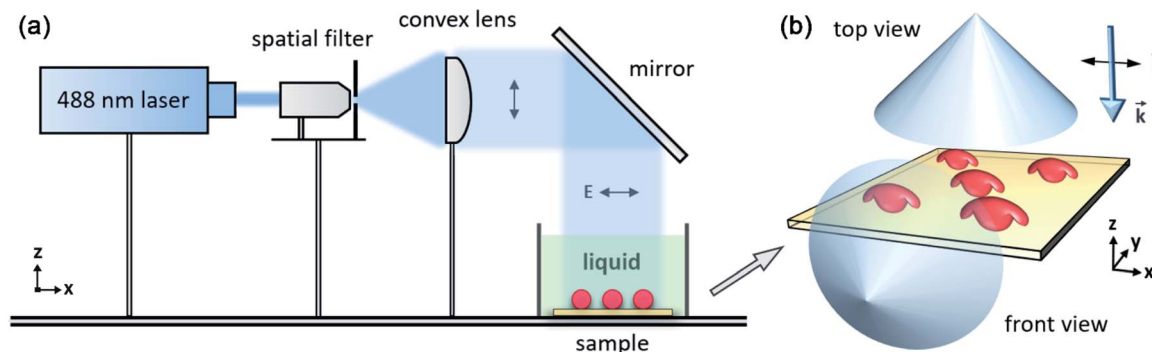
Fig. 1 (a) Experimental setup for investigating the photoinduced deformation of IAC-4 microspheres in the aqueous medium. (b) Schematic diagram of the morphology characterization of the deformed particles from the top-view and the front-view. The Cartesian coordinate system is indicated in each figure.

photoinduced deformation patterns,[39,40] which is favorable for investigating the mechanisms of the mass transfer and for demonstrating unique functionalities as well. The experimental setup used here is illustrated in Fig. 1a, where the IAC-4 microspheres were loaded on a piece of the silicon substrate immersed in an aqueous medium. The substrate was pre-coated with a thin sticky layer of PBA that could tightly immobilize the IAC-4 microspheres on the substrate when immersed in the aqueous medium (Fig. S7 in ESI†). The microspheres were illuminated by a collimated and linearly polarized laser beam (λ = 488 nm) with the homogeneous intensity of 200 mW cm^{-2} at normal incidence. After being irradiated for a period of time and then properly dried, the asymmetric morphologies of the photo-deformed particles were characterized by SEM from two orthogonal directions (the top-view and front-view, Fig. 1b) to uncover the photoinduced mass transfer behavior. The top-view SEM was taken in the direction of the propagation of the laser beam (the negative z direction), which tells the shape variation in the x–y plane. The front-view SEM was taken along the y-axis, which was orthogonal to both the propagation direction (the $-z$ axis) and the electric vibration direction (the x-axis) of the

polarized light, and it presents the morphologic changes in the x–z plane. In addition, the reflection-mode OM observations from the top-view were adopted to quantitatively characterize the anisotropic flattening of the upper part of the particles. Through these ways, the photoinduced mass transfer behavior of IAC-4 microspheres in various immersion media, including water and aqueous solutions with different refractive indices and viscosities, was systematically studied by examining the morphologies of the deformed particles and comparing with that obtained in the air-ambient condition (the control). Optical analysis and calculation were also conducted to provide a deep understanding of the mechanism as discussed below in details.

Effect of aqueous immersion medium

Before the light irradiation, the IAC-4 microspheres exhibit the uniform spherical shape and monodispersed size, as verified by the top-view SEM images (Fig. 2a and b, captured with different magnifications). After the linearly polarized light irradiation in air for 1 h (Fig. 2c and d), the microspheres were significantly elongated along the electric vibration direction of the polarized
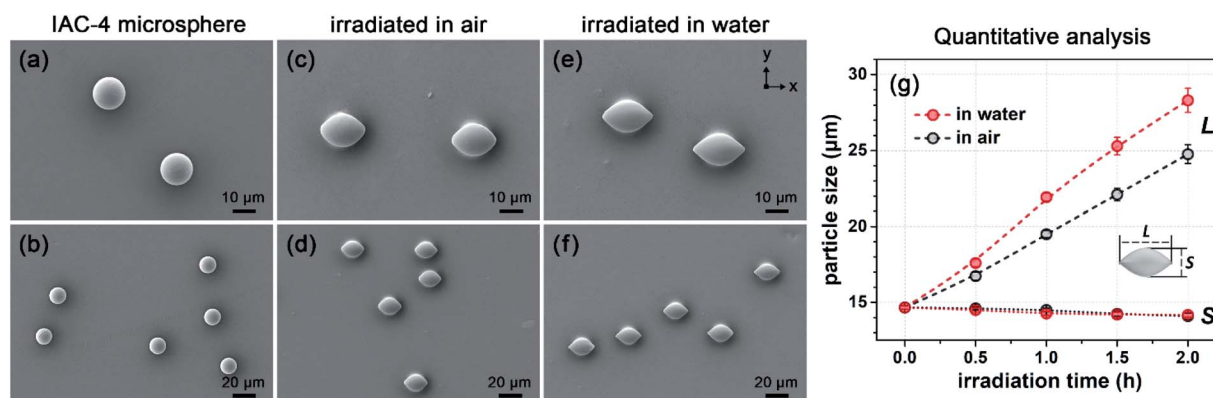

Fig. 2 (a–f) Top-view SEM images of the IAC-4 particles, (a and b) the microspheres before irradiation, (c–f) the deformed particles after linearly polarized light irradiation for 1 h in air (c and d) and in water (e and f). The images in (a, c and e) and (b, d and f) were respectively captured with two different magnifications. The coordinate system is indicated in (e), which can be applied to the other panels. (g) Variation of the anisotropic dimensions (L and S) of the deformed particles after irradiated in air (gray color) and water (red color) for the different time periods. The definition of L and S is illustrated in the inset of (g).

light (parallel to the *x*-axis), and the deformed particles exhibit the spindle-like morphologies from the top-view. The photoinduced elongation is originated from the directional mass transfer of azobenzene-containing materials, which has been well documented in the literature.[37–45] To our surprise, the IAC-4 microspheres immersed in water generate a more significant deformation upon the irradiation with the same light intensity (Fig. 2e and f). To quantitatively compare the deformation degrees in air and water, we measured the sizes along the long axis (*L*) and short axis (*S*) of the spindle-like structures in the top-view SEM images. The averaged sizes, obtained from the statistics of at least 30 particles for each data point, are shown in Fig. 2g as a function of the irradiation time. Benefited from the monodispersed size of microspheres and the stable intensity of laser, the photo-deformed particles exhibit uniform shapes (Fig. 2c–f) and small deviations (seen form the error bars in Fig. 2g), which ensures the accuracy and reliability of the measurements. For the same irradiation period, the IAC-4 microspheres immersed in water show the obviously larger elongation along the long axis (*L*) than that obtained in air, which indicates an enhanced mass transfer efficiency in this direction. The mean elongation rate ($\Delta L/\Delta t$) within the irradiation period of 2 h is calculated to be 7 μm h^{-1} for that obtained

in water medium, 1.4-fold of that obtained in air (4.9 μm h^{-1}). On the other hand, the shrinkage along the short axis (*S*) of the particles is much smaller and the difference between these two compared cases is negligible (Fig. 2g). It indicates that except the change results from the photoinduced mass transfer, the water immersion medium does not cause the shape variation by swelling or other effects.

Above result shows that by employing water as the immersion medium, the particles with larger shape-anisotropy (characterized by *L/S*), compared with that obtained in air, can be photo-fabricated under the same irradiation condition. It has reason to believe that the difference is caused by the higher refractive index of water (1.333) relative to that of air (1). To confirm this point, the photoinduced mass transfer in an immersion medium with a higher refractive index than water was tested. The KSCN solution (70 wt%) with the higher refractive index (1.491) was selected as the immersion medium. This inorganic salt solution is a colorless liquid with the low viscosity,[55] low density and high optical transparency (nearly 100%) resemble to deionized water (Table S1 and Fig. S5 in ESI†). Moreover, it does not corrode or swell the IAC-4 microspheres (Fig. S7 in ESI†). Fig. 3a–d show the front-view SEM images of the photo-deformed particles after irradiation for
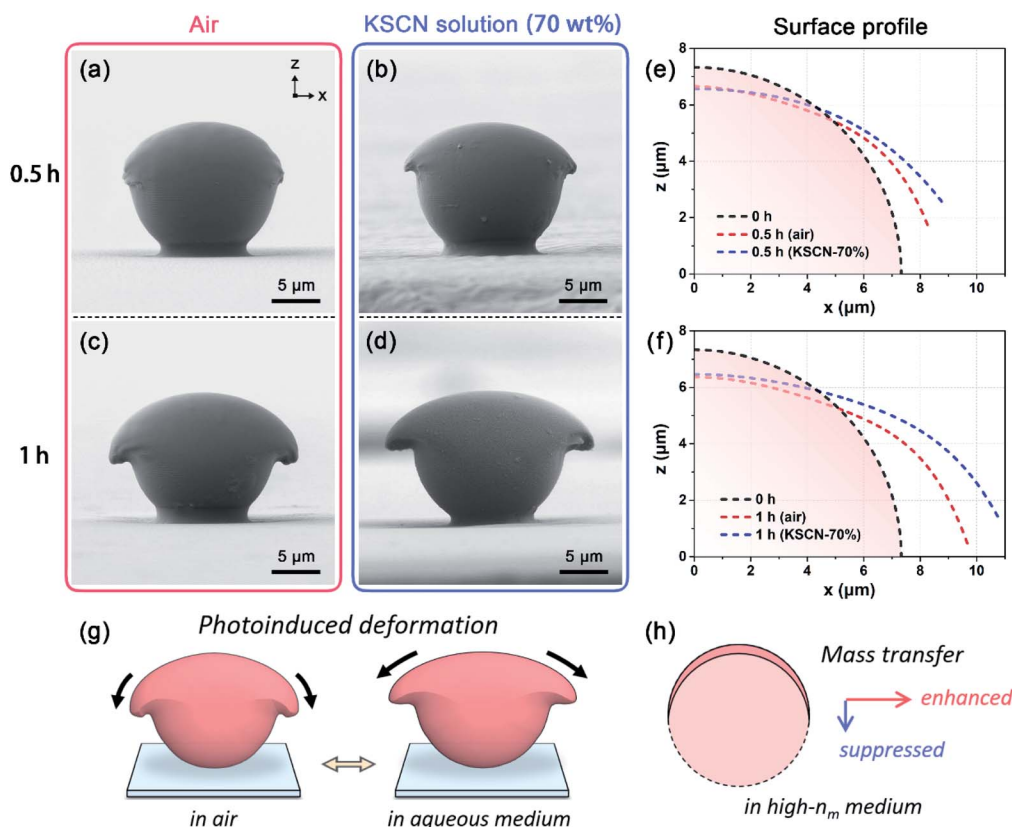

Fig. 3 (a–d) Front-view SEM images of the photo-deformed IAC-4 particles after irradiation with linearly polarized light, (a and b) for 0.5 h, (c and d) for 1 h, (a and c) air-ambient, (b and d) immersed in the KSCN solution (70 wt%). The Cartesian coordinate system is indicated in (a), which can be applied to the other panels. (e and f) Upper surface profiles (right half) of the *xOz* cross-section of the deformed particles after laser irradiation for (e) 0.5 h and (f) 1 h, compared with the surface profile of the microsphere before irradiation. (g) Schematic illustration of the effect of the aqueous medium on tuning the photoinduced deformation direction. (h) Schematic illustration of the effect of n_{me} on the mass transfer behavior in the two orthogonal directions.

0.5 h and 1 h in air and the KSCN solution (70 wt%), where the image of the original IAC-4 microspheres can be seen in Fig. S8 (in ESI†). As the top-view SEM images given in Fig. 2 only show the deformations viewed from one direction, the front-view SEM images are shown here to give a comprehensive view of the deformations. The mushroom-like morphologies of the deformed particles indicate that the photoinduced deformation mainly occurs on the upper parts of the particles. This phenomenon is originated from the strong optical absorption ability of IAC-4 (Fig. S4†).[40] Under the 488 nm light irradiation, the upper surface layer with a thickness less than 1 μm absorbs most of the incident light and the significant mass transfer only occurs in this part, while the inner part and lower half of the ten-micron-sized microsphere show no observable deformation. As revealed in Fig. 3c and d, the immersion medium does not obviously influence the deformation region, while it significantly changes the deformation direction of the upper surface parts. In the air-ambient condition (Fig. 3c), the upper part of microsphere is not only elongated parallel to the x-axis but also bent towards the substrate (deformed in the $-z$ direction) to a larger extent, indicating the mass transfer can be decomposed to the migrations in these two directions. When the microsphere is irradiated in KSCN solution (70 wt%), although the shape elongation parallel to the x-axis is significant, the deformation in the $-z$ direction is reduced (Fig. 3d). Compared with the former case (Fig. 3c), the upper cap of the mushroom-like particle in Fig. 3d is more extended parallel to the substrate plane, but shows a less bending curvature towards the substrate.

To give a more convincing comparison, the front-view SEM images of IAC-4 microsphere (Fig. S8 in ESI†) and deformed particles (Fig. 3a–d) are compared by their surface profiles (Fig. 3e and f). The microsphere center is defined as the origin $O(0,0,0)$, and the outlines thus correspond with the surface profiles in the xOz cross-section of the particles. For the irradiation time of 0.5 h (Fig. 3e) and 1 h (Fig. 3f), the upper parts show the larger deformations parallel to the substrate (the x-axis) and smaller deformation towards the substrate (the $-z$-axis) in the KSCN solution compared with those obtained in air. It means that the employment of the aqueous medium enhances the mass transfer parallel to the x-axis and reduces that in the $-z$ direction. In other words, the aqueous solution tunes the deformation direction by modifying the mass transfer scales in these two directions (Fig. 3g and h). Our previous work shows that the light refraction at the interface between air and the microsphere can generate the z-component of the electric field vibration of the transmitted wave, which drives the mass transfer in the $-z$ direction.[40] Therefore, adjusting the refractive index of the immersion medium (n_{me}) can cause the obvious change of the photoinduced mass transfer behavior. The effect of n_{me} can be more clearly seen by the reflection-mode OM as discussed in the following section.

Quantitative characterization of photo-induced mass transfer

As shown in Fig. 3e and f, the surface curvatures of the deformed particles are obviously different when irradiated with the polarized light in the aqueous immersion medium, compared with that obtained in the air-ambient condition. However, as the observation direction of the front-view SEM is parallel to the substrate plane, particles could be clearly imaged only one at a time, and it is difficult to carry out statistics requiring a large amount of imaged samples. Therefore, we established a more satisfactory method based on the reflection-mode optical microscopy (OM) to quantitatively characterize both the anisotropic shapes and surface curvatures of photo-deformed particles obtained in different conditions.

In the reflection-mode OM, the light source illuminates the IAC-4 particles from above (for the top-view), and the objective lens collects the light reflected from the upper surface to form the image. As illustrated in Fig. 4a, the specular reflection light from the top region (the white color) of the microsphere can be collected by the lens and projected to the image plane. This region is shown as a circular bright spot homocentric to each microsphere in the OM image (Fig. 4b), where the white color is attributed to the signal saturation of CCD caused by the high reflectivity. On the other hand, the specular reflection light on the peripheral region of microsphere (the red color part in Fig. 4a) is beyond the maximum collectable light cone of the objective lens. This region is imaged solely through the diffusion reflection with a lower reflectivity, which presents the red color in OM image (Fig. 4b) due to the selective optical absorption of IAC-4 (Fig. S4 in ESI†). For the objective lens operated in air (without oil immersion), the half-angle of the maximum collectable light cone (θ_c) is determined by the numerical aperture (NA),[56,57]

$$\sin(\theta_c) = \sin(2\theta_{in}) = NA \qquad (1)$$

where θ_{in} is the incident angle on the edge of bright spot (Fig. 4a). In our experiment, NA of the objective lens was 0.55,
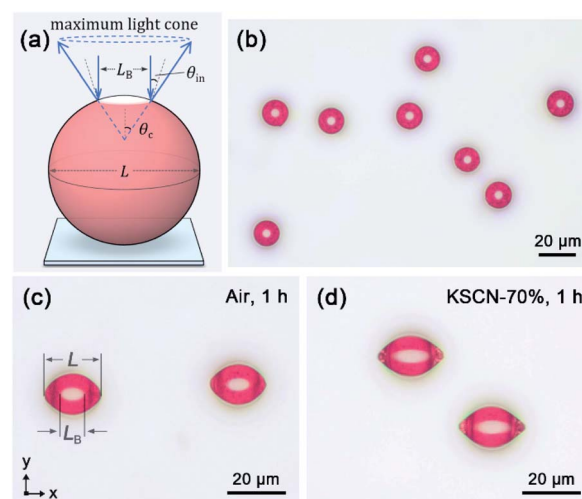

Fig. 4 (a) Schematic illustration about the formation of the bright spot in OM images. (b–d) Reflection-mode OM images, (b) the IAC–4 microspheres before the light irradiation, (c) the deformed particles after linearly polarized light irradiation for 1 h in air, (d) in the KSCN immersion medium (70 wt%). The Cartesian coordinate system and the definitions of L and L_B are indicated in (c).

and θ_{in} was calculated to be 16.7°. For the spherical surface (see the illustration in Fig. 4a), the length of bright spot (L_B) and the diameter of microsphere (L) are correlated with θ_{in} following the relationship,

$$(L_B/L)_{sphere} = \sin(\theta_{in}) \qquad (2)$$

According to our measurements, L_B/L of the IAC-4 microspheres in OM images shows the averaged value of 0.293 ± 0.004, well agrees with the theoretical prediction ($\sin(\theta_{in}) = 0.287$). Consequently, the bright spot corresponds with a relatively flat region on the upper surface of a microsphere, where the incident angle (the intersection angle between the normal of microsphere surface and the normal of substrate) is less than $\theta_{in} = 16.7°$. Noteworthy, this criterion is also valid for the photo-deformed particles with non-spherical surfaces, which is proved in Section 5.2 in ESI.†

Fig. 4c and d show the reflection-mode OM images of the photo-deformed particles after the linearly polarized light irradiation in air and the KSCN solution for 1 h, where the particles obtained in the liquid immersion condition was properly rinsed and dried before the observation. Accompanied with the photoinduced shape elongation, the bright spots are also significantly stretched parallel to the x-axis and transformed into the spindle-like shapes, which are more obvious for the irradiation in the KSCN immersion medium (Fig. 4d) than those obtained in the air-ambient condition (Fig. 4c). As the bright spot represents a relatively flat surface region of a particle, its size expansion upon irradiation reveals the directional surface flattening of the IAC-4 microspheres caused by the mass transfer. Quantitatively, the surface flattening degree of deformed particles can be characterized by L_B/L, i.e., the size ratio between the flat region and the whole particle in the x-axis, as illustrated in Fig. 4c. For the spherical surface and a planar surface, L_B/L is 0.287 and 1, respectively. The L_B/L values of photo-deformed particles increase with the irradiation time (Fig. S9†), which are quantitatively correlated with the surface flattening process upon the polarized light irradiation.

By this method, the photoinduced deformation and surface flattening of IAC-4 microspheres were investigated upon the light irradiation in air, water and KSCN solutions (30 wt%, 52 wt% and 70 wt%). These surrounding environment and media show an ascending order of refractive index (n_{me}) from 1, 1.333, 1.394, 1.448 to 1.491. The length of the deformed particle (L), the length of bright spot (L_B) and their ratio (L_B/L), which respectively reflect the photoinduced deformation parallel to the x-axis, the size expansion of top flat region and the surface flattening degree, were measured from the OM images and averaged from the statistics of at least 30 particles. The results indicate that as n_{me} increases from 1 to 1.491, L, L_B, and L_B/L all gradually increase for the irradiation time of 1 h for instance (Fig. 5). The measurements for a shorter irradiation time of 0.5 h are given in Fig. S10 (in ESI†), which appear similar to the above results. The positive correlation between n_{me} and the deformation scale parallel to the x-axis (Fig. 5a) coincides with the top-view SEM observation (Fig. 2g). As shown in Fig. S11 (in
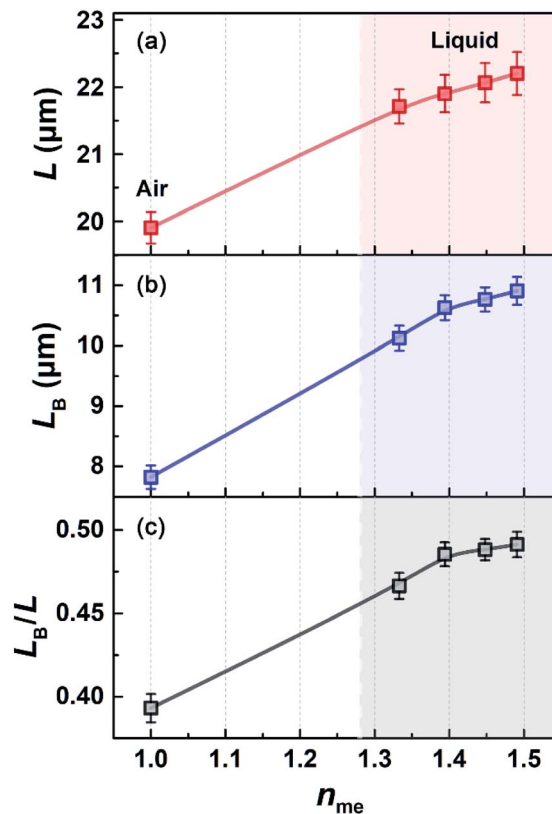

Fig. 5 (a) L, (b) L_B and (c) L_B/L of the photo-deformed particles after the linearly polarized light irradiation for 1 h, plotted *versus* the refractive index of the immersion medium (n_{me}).

ESI†), these two characterization methods are highly consistent with each other. On the other hand, the reflection-mode OM can supply information of the surface flattening, which could not be obtained by the top-view SEM. Considering L of the deformed particle and L_B of the bright spot are both measured along the long axes (Fig. 4c), the ratio L_B/L represents the flatness of the surface profile in the xOz plane. The larger value of L_B/L observed in the high-n_{me} medium (Fig. 5c), i.e., the reduced curvature of the surface in the xOz cross-section, corresponds to the enhanced mass transfer parallel to the x-axis and the reduced mass transfer scale in the $-z$ direction. These results were also observed from the upper surface profiles for the xOz cross-section of the photo-deformed particles (Fig. 3e and f), both of which are highly consistent with each other.

Influence of viscosity of aqueous immersion medium

The above results demonstrate that the photoinduced mass transfer behavior of the IAC-4 microspheres in the aqueous immersion media is quite distinct from that observed in the air-ambient environment. For a liquid immersion medium, the viscosity could be an important factor to influence the mass transfer behavior. Water used as the immersion medium has the viscosity of 0.797 mPa s.[58] In order to investigate the possible influence of the medium viscosity (η_{me}), three PVA immersion media (2.5 wt%, 5 wt% and 8 wt%) with η_{me} of 9.316,

89.87 and 791.5 mPa s were adopted, which are much higher than that of water. On the other hand, the immersion media possess the similar refractive indices with deionized water (Table S1, ESI†) and exhibit high optical transparency (nearly 100%) in the visible light region (Fig. S5a, ESI†), which can avoid the possible influences of these factors.

Fig. 6a and b show the front-view SEM images of the photo-deformed particles after the linearly polarized light irradiation for 0.5 h with water and the PVA solution (5 wt%) as the immersion media. Even in the highly viscous liquid, the photoinduced mass transfer can still occur for the upper part of microsphere. As the mushroom-like particles in Fig. 6a and b show nearly the same morphology, it has reason to believe that the mass transfer scale and direction are not affected by η_{me}. The mass transfer scale and direction were quantitatively characterized by the deformation and surface flattening of the microspheres after the irradiation with water and three PVA solutions as the immersion media and in air as well. The parameters (L, L_B and L_B/L) were obtained from the reflection-mode OM images, where two typical OM images are shown in Fig. 6c and d. As shown in Fig. 7, these parameters of the deformed particles obtained in the aqueous immersion media (the right colored region in Fig. 7) are all larger than those obtained in air. However, for the four aqueous media with η_{me} covering three orders of magnitude, the deformation efficiency parallel to the x-axis (Fig. 7a), the size expansion of top flat region (Fig. 7b) and the surface flattening degree (Fig. 7c) are the same within admissible errors. These results quantitatively prove that the viscosity of the immersion media has no detectable influence on the mass transfer behavior. The results given in Fig. 7 also indicate that other factors related to viscosity variation of the immersion media, such as coefficients of
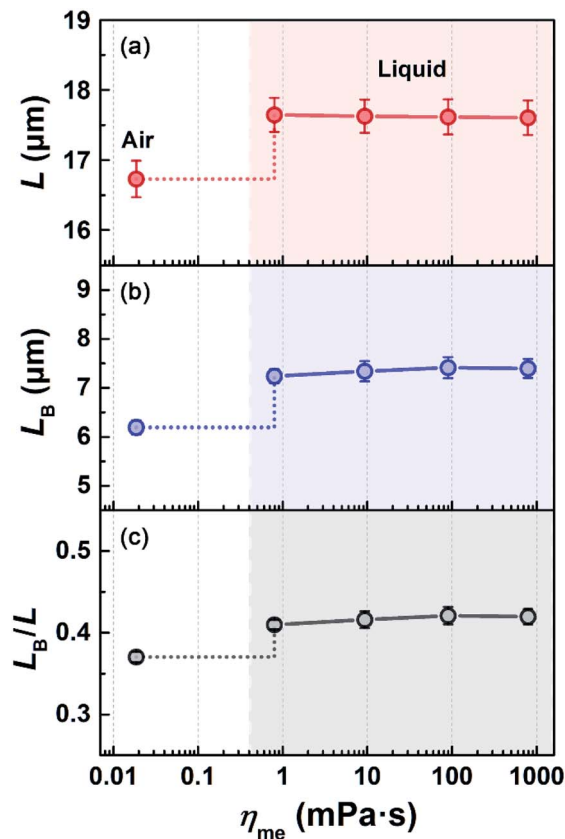

Fig. 7 (a) L, (b) L_B and (c) L_B/L of the photo-deformed particles after the linearly polarized light irradiation for 0.5 h, plotted *versus* the viscosity of medium (η_{me}).

thermal conductivity and diffusion, show no detectable influence. All these variations related to the transport environment at the interface and in the media seem to have no influence on the mass transfer behavior. One common characteristic of the above aqueous media is that their n_{me} values are in the same range (from 1.333 to 1.345). The photoinduced mass transfer behavior in these immersion media appears to be the same, as characterized by the shape elongation (Fig. 7a) and the surface flattening degree (Fig. 7c) of the deformed particles, but is obviously different than that obtained in air ($n_{me} = 1$). This result is accordant with the results presented in the above sections. The mechanism behind the unique effect of n_{me} will be discussed in the following section.

Effect of aqueous media on refracted light in microsphere

To understand the effect of the refractive index of the immersion media, the propagation direction of refracted light and electric field energy distribution at the interface of IAC-4 microspheres with the media were analyzed by the optical calculation. The xOz cross-section showing the most significant deformation of the microsphere was selected for the calculation. As shown in Fig. 8a, the propagation of the 488 nm linearly polarized light is represented by a unit vector $\mathbf{k}_0$ in the $-z$ direction and the electric field $\mathbf{E}_0$ in the x-axis. Due to the normal incidence at the air–medium interface, the light
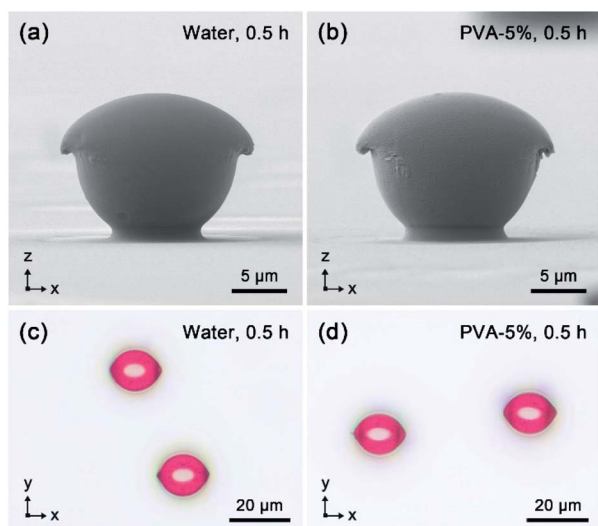

Fig. 6 (a and b) Front-view SEM images and (c and d) reflection-mode OM images of the photo-deformed particles after linearly polarized light irradiation in (a and c) deionized water and (b and d) PVA solution (5 wt%) for 0.5 h. The Cartesian coordinate systems are labeled in each panel. The images were taken after rinsed with deionized water and dried in ambient conditions.
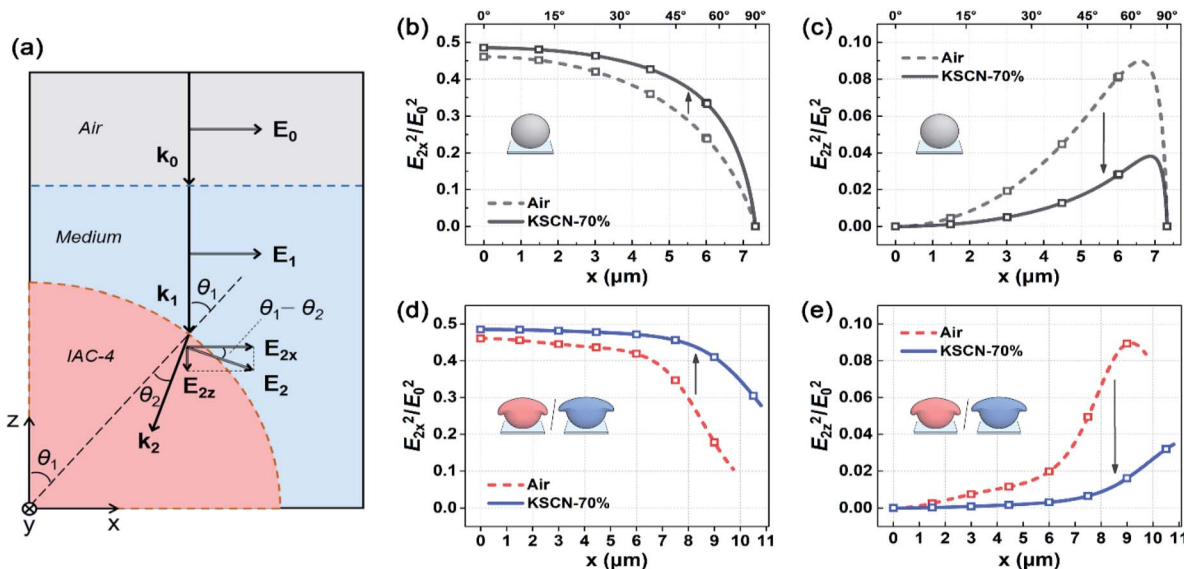
Fig. 8 (a) Schematic illustration about the light refraction and electric field variation at the microsphere interface, where **k** and **E** respectively represents the propagation direction and electric field of the light. (b) $E_{2x}{}^2$ and (c) $E_{2z}{}^2$ at the interface between medium and IAC-4 microsphere *versus* x upon light irradiation in air and KSCN solution (70 wt%). The values were normalized with $E_0{}^2$, and the incident angle (θ_1) on the microsphere surface is plotted on the top. (d) $E_{2x}{}^2$ and (e) $E_{2z}{}^2$ at the interface between the medium and the deformed particles *versus* x after the light irradiation in air and KSCN solution (70 wt%) for 1 h. The calculation used the cross-sectional profiles shown in Fig. 3f.

propagation direction (represented by the unit vector $\mathbf{k}_1$) and electric field ($\mathbf{E}_1$) in the immersion medium are parallel to $\mathbf{k}_0$ and $\mathbf{E}_0$. At the curved upper surface of the microsphere, the light is refracted at the medium–microsphere interface and the refracted light (*i.e.* transmitted into the microsphere) has the electric field ($\mathbf{E}_2$) with the x-component ($\mathbf{E}_{2x}$) and z-component ($\mathbf{E}_{2z}$). As the diameter of microsphere (*ca.* 14 μm) is much larger than the light wavelength ($\lambda = 488$ nm), the light refraction is calculated by Snell's law,[56]

$$n_{\text{me}} \sin(\theta_1) = n_{\text{azo}} \sin(\theta_2) \tag{3}$$

where θ_1 and θ_2 are the incident angle and refracted angle at the medium–microsphere interface, and n_{azo} is the refractive index (the real part) of IAC-4. Measured by ellipsometry, n_{azo} is 1.946 at the wavelength of 488 nm (Fig. S4†), which is larger than all n_{me} values used in this work. Therefore, according to eqn (3), θ_2 is smaller than θ_1 (Fig. S12 in ESI†). The angle $\theta_1 - \theta_2$ defines the deviation of the propagation direction ($\mathbf{k}_2$) of the transmitted light from the $-z$ direction, which is also the intersection angle between $\mathbf{E}_2$ and the x-axis, as illustrated in Fig. 8a. The amplitude of $\mathbf{E}_2$ (*i.e.*, the amplitude of transmitted electric field at the microsphere surface) is calculated by,

$$\mathbf{E}_2 = t_{21} \times t_{10} \times E_0 = \frac{2n_{\text{me}} \cos(\theta_1)}{n_{\text{azo}} \cos(\theta_1) + n_{\text{me}} \cos(\theta_2)} \frac{2}{1 + n_{\text{me}}} E_0 \tag{4}$$

where E_0 is the amplitude of the electric field of the incident light in air. The amplitude transmission coefficients, $t_{21} = E_2/E_1$ for the medium–microsphere interface and $t_{10} = E_1/E_0$ for the air–medium interface, are obtained using Fresnel law.[56] The detailed procedure is given in ESI.† Due to the reflection at the interfaces, t_{21} and t_{10} are both less than 1, whose values depend

on n_{me}. By decomposing $\mathbf{E}_2$ into the x- and z-components, the amplitudes of $\mathbf{E}_{2x}$ and $\mathbf{E}_{2z}$ are obtained,

$$\mathbf{E}_{2x} = \frac{2n_{\text{me}} \cos(\theta_1)}{n_{\text{azo}} \cos(\theta_1) + n_{\text{me}} \cos(\theta_2)} \frac{2}{1 + n_{\text{me}}} \cos(\theta_1 - \theta_2) E_0 \tag{5}$$

$$\mathbf{E}_{2z} = \frac{2n_{\text{me}} \cos(\theta_1)}{n_{\text{azo}} \cos(\theta_1) + n_{\text{me}} \cos(\theta_2)} \frac{2}{1 + n_{\text{me}}} \sin(\theta_1 - \theta_2) E_0 \tag{6}$$

As the light intensity is proportional to the square of electric field amplitude, $E_2{}^2$, $E_{2x}{}^2$ and $E_{2z}{}^2$ represent the intensity of transmitted light and its energy distributions in the x- and z-directions at the medium–microsphere interface. According to eqn (4)–(6), there is a relationship $E_{2x}{}^2 + E_{2z}{}^2 = E_2{}^2$ and $E_0{}^2$ has a constant value as the light intensity was fixed (200 mW cm^{-2}) in the experiments.

Fig. 8b and c show $E_{2x}{}^2$ and $E_{2z}{}^2$ at the medium–microsphere interface *versus* x ($x = R \sin \theta_1$, R = microsphere radius) upon light irradiation in air ($n_{\text{me}} = 1$) and KSCN solution (70 wt%, $n_{\text{me}} = 1.491$). The calculation results for other immersion media with the different n_{me} values are shown in Fig. S13 in ESI.† The result indicates that the increase of n_{me} (from 1 to 1.491) causes a significant increase of $E_{2x}{}^2$ (Fig. 8b and S13b in ESI†) and decrease of $E_{2z}{}^2$ (Fig. 8c and S13c in ESI†) at the medium-microsphere interface. Consequently, the mass transfer parallel to the substrate (the x-axis) is enhanced and that towards the substrate (the $-z$ axis) is reduced in the aqueous immersion media with the high n_{me} values. According to eqn (4)–(6), the influences of n_{me} on $E_{2x}{}^2$ and $E_{2z}{}^2$ include two parts, *i.e.*, $t_{21}t_{10}$ and $\theta_1 - \theta_2$, which represent the optical transmittivity through the two interfaces and the refraction at the medium–microsphere interface, respectively. Firstly, as the refractive

indexes of the aqueous immersion media are between air and IAC-4 ($n_{air} < n_{me} < n_{azo}$), the media play a role of refractive-index matching layer between the air and microsphere, which reduces the overall reflection loss at the interfaces and increases the transmittivity. As shown in Fig. S13a (in ESI†), the ratio E_2^2/E_0^2, equal to $(t_{21}t_{10})^2$, shows a slight increase with n_{me}, indicating the more light energy can be received by the microsphere through the high-n_{me} medium. However, this effect is less important compared with the effect of the $\theta_1 - \theta_2$ variation. In fact, the distinct light refraction behavior at the microsphere interface in different immersion media is the crucial factor to affect the mass transfer. As shown in Fig. S12b (in ESI†), with increasing n_{me} (decreasing the difference with n_{azo}), $\theta_1 - \theta_2$ is obviously decreased and the travelling direction of the refracted light ($\mathbf{k}_2$) is closer to the $-z$ axis (the direction of $\mathbf{k}_0$). As the light is a transverse wave, the vibration direction of $\mathbf{E}_2$ is then closer to the x-axis (the direction of $\mathbf{E}_0$), which causes the increased x-component ($\mathbf{E}_{2x}$) and the reduced z-component ($\mathbf{E}_{2z}$). Consequently, E_{2x}^2 of the refracted light is obviously larger for the microsphere and deformed particle in the aqueous immersion media than that in air, where E_{2x}^2 is more sensitive to the n_{me} increase than E_2^2 (Fig. S13a and b in ESI†). The calculation of the deformed particles shows the similar results (Fig. S14 and S15 in ESI†).

Discussion

The morphological characterizations by the top-view SEM, the front-view SEM and the reflection-mode OM comprehensively demonstrate that the photoinduced mass transfer behavior of the IAC-4 microspheres in the aqueous immersion media is distinct from that observed in the air-ambient condition. Under the same irradiation condition (wavelength, intensity and irradiation time), employing an aqueous medium with larger n_{me} enhances both the shape elongation (Fig. 2g and 5a) and the surface flattening (Fig. 3e, f and 5c) of the IAC-4 microspheres. The variations result from the enhanced mass transfer parallel to the x-axis and the reduced mass transfer in the $-z$ direction caused by the increased n_{me} (Fig. 3g and h). To the best of our knowledge, this effect of the immersion medium and its mechanism have not been reported in the literature yet.

Based on above calculation, the effect caused by the immersion media can be attributed to the variation of the light refraction behavior at the medium–microsphere interface. It has been well documented that the photoinduced mass transfer of azo polymer and molecular glass in air-ambient environment occurs along the direction of the electric vibration of the polarized light.[12–21] Based on the observations of the current study and above calculation, we argue that in the aqueous media, the photoinduced mass transfer also occurs in the direction of the electric vibration of the polarized light. In the medium with the larger n_{me}, the mass transfer along the vibration direction of $\mathbf{E}_2$ occurs in a direction closer to the x-axis, i.e. it shows less deformation towards the substrate (Fig. 3g). The results given in Fig. 2–5 can be well explained by considering the variations of E_{2x}^2 and E_{2z}^2 (Fig. 8b and c). According to the calculation results (Fig. S16 in ESI†), E_{2x}^2 and

E_{2z}^2 of the refracted light are rapidly attenuated with the travelling distance in the microsphere due to the strong optical absorption of IAC-4. The light penetration depth is much smaller than the microsphere diameter and is not affected by n_{me} variation, which agree well with the scales of deformation regions observed from the front-view SEM (Fig. 3a–d). For the refracted light in the microsphere, the direction of the electric vibration is not changed, while the amplitude rapidly declines to 0 in the upper layer of the microsphere (Fig. S16 in ESI†). Therefore, E_{2x}^2 and E_{2z}^2 at the microsphere surface represent the light energy absorbed by IAC-4 in the unit time to cause the mass transfer in the x and $-z$ directions. As shown in Fig. 8b and c, the E_{2x}^2 increase and E_{2z}^2 decrease can be more clearly seen for the angle θ_1 in the range from 30–70°, which controls the morphology of the deformed particles. As a consequence, after the light irradiation for a same time period, the photodeformed particles obtained in the aqueous medium possess the flattened upper surface (Fig. S14b and d in ESI†), compared with those obtained in the air-ambient condition (Fig. S14a and c in ESI†). As shown in Fig. 8d and e, upon light irradiation in the KSCN solution (70 wt%) for 1 h, the tendency of E_{2x}^2 increase and E_{2z}^2 decrease can also be seen for the deformed particles, compared with those obtained in the air-ambient condition. For a shorter irradiation time of 0.5 h, the similar result can be observed (Fig. S15 in ESI†). These calculations can rationalize the observations that the aqueous media enhance the shape deformation parallel to the x-axis and supply some deep understanding. Although using longer irradiation time under ambient air can produce particles with different shapes,[39] the deformations similar to those in the aqueous immersion media can hardly be produced due to the variations of E_{2x}^2 and E_{2z}^2 caused by the media.

Except the effect of refractive index discussed above, the observations of this study also give other important insights into the mass transfer process. The thermal dissipation through a liquid is much more efficient than that of air due to the higher coefficient of thermal conductivity and higher heat capacity. Therefore, the photo-thermal effect can be avoided and negligible in the aqueous immersion media compared that under the air-ambient condition. By using different types of aqueous media, i.e., deionized water, KSCN solutions with different concentrations and PVA solutions with different concentrations, the properties such as viscosity, density (Table S1 in ESI†), coefficient of thermal conductivity and coefficient of diffusion are considerably altered. However, these variations show no detectable influence on the photoinduced mass transfer behavior. This confirms that the mass transfer is solely caused by the light and this effect is not sensitive to the transport conditions at the medium–microsphere interface and in medium.

Photoinduced deformation of IAC-4 microarrays in water

In the above sections, the ten-micron-sized IAC-4 microspheres were employed as a substance to investigate the photoinduced mass transfer in various aqueous media. For the microspheres, the spherical surface covers the full range

of incident angle (0–90°), and the large size restricts the deformation to solely occur in the upper region. These features are helpful to elucidate the mass transfer behavior related to the light refraction at the medium–microsphere interface. In this part, we further prove that the understanding of the effect of the immersion medium is not limited to this specific type of structures. To demonstrate the applicability to other cases, the photoinduced deformation in the water immersion medium was tested using the submicron-sized pillar arrays (Fig. 9a) and hole arrays (Fig. 9b) of IAC-4, which show the periodic structures arranged in the hexagonal lattice. The IAC-4 microarrays were fabricated by a soft-lithography hot-embossing method,[16] and the procedure is described in ESI.† The light irradiation setup was the same as that used for IAC-4 microspheres (Fig. 1a), except the light intensity (after the 45° mirror) was set to be 20 mW cm^{-2} as the sizes of the topographic structures were much smaller. Fig. 9c–f show the top-view SEM images of the pillar and hole microarrays after the irradiation with the linearly polarized light (488 nm) in air and deionized water for 8 min. SEM images of the structures after the light irradiation for different time periods are shown in Fig. S17 in ESI.†

As shown in the images, the circular cross-sections of the cylindrical pillars are transformed into the elliptical shapes aligned parallel to the x-axis due to significant elongation parallel to the electric vibration direction of incident light (Fig. 9c and e), while the round holes were contracted in this direction and transformed into the elliptical holes aligned parallel to the y-axis (Fig. 9d and f). These anisotropic deformations are both originated from the directional mass transfer of IAC-4, while the different morphologies are attributed to the distinct deformation patterns of the pillars and holes (Fig. S18

in ESI†). Although these variations can be seen for both air and water medium, the IAC-4 microarrays in the water immersion medium (Fig. 9e and f) show the more significant deformation in the x–y plane and exhibit the larger shape-anisotropy than that obtained in the air-ambient condition (Fig. 9c and d) under the same irradiation condition. This observation is further confirmed by the quantitative measurements of the aspect ratio (L/S) of the photo-deformed microarrays obtained at different irradiation periods (Fig. S19, in ESI†). The effect of the water immersion medium to enhance the photoinduced deformation coincides with that observed for the ten-micron-sized IAC-4 microspheres. As discussed above, the aqueous medium with larger n_{me} than air decreases $\theta_1 - \theta_2$ value at the interface between the medium and the ten-micron-sized particles, which increases the E_{2x}^2 and enhances the mass transfer efficiency in the x-axis. Concerning that the structural sizes of IAC-4 pillars/holes in the arrays are in the same order of magnitude with the light wavelength ($\lambda = 488$ nm), the above light refraction theory cannot be applied mechanically. On the edges of the submicron-sized structures, the light diffraction and scattering can cause the depolarization effect and other changes.[3,31,56] Compared with air, water shows a smaller refractive-index difference with IAC-4 ($n_{air} < n_{me} < n_{azo}$), which both reduces the reflection loss on the interfaces and weakens the depolarization effect on the edges. As more light energy was received by the IAC-4 microarrays in water medium to generate the mass transfer along the electric vibration of incident light (in the x-axis), the more significant shape variations in x–y plane were thus observed. Therefore, it is proved that the photo-fabrication based on the mass transfer in aqueous immersion medium is not limited to the microspheres and can be applied to many other cases.
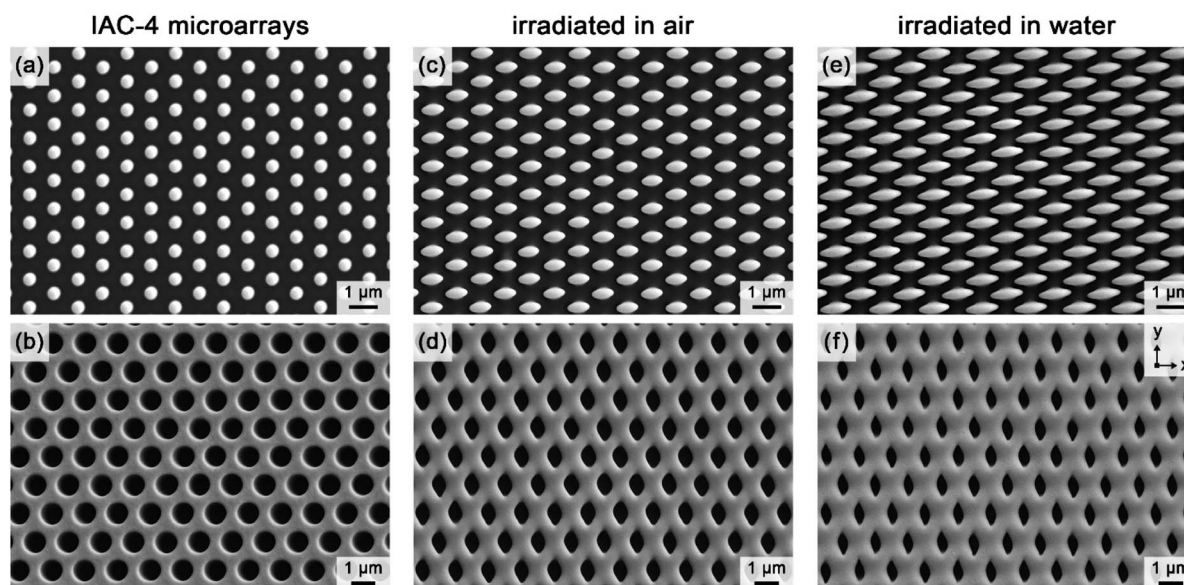

Fig. 9 Top-view SEM images of the IAC-4 structures, (a) micron-pillar arrays, (b) micron-hole arrays fabricated by soft-lithography. Top view SEM images of the IAC-4 microarrays after the 488 nm linearly polarized light irradiation in air (c and d), in deionized water (e and f) for 8 min. Light intensity was fixed to be 20 mW cm^{-2} for each case. The Cartesian coordinate system is indicated in (f), which can be applied to the other panels.

Conclusions

In summary, the photoinduced mass transfer of ten-micron-sized IAC-4 microspheres was investigated in water and other aqueous solutions to understand the effects of the immersion media on this intriguing process caused by polarized light irradiation. In contrast to the conventional air-ambient cases, the light irradiation was carried out in the deionized water, KSCN solutions with different refractive indices (n_{me}) and the PVA solutions with different viscosities (η_{me}) as the immersion media. Upon the linearly polarized light irradiation at 488 nm for a period of time, the IAC-4 microspheres immersed in these media (water and aqueous solutions) all manifested significant shape deformation through the directional mass transfer. The photo-deformed particles with the asymmetric morphology and anisotropic dimension were characterized by SEM from two orthogonal views (the top-view and front-view) to uncover the shape evolution and mass transfer behavior in different immersion media, which were compared with those obtained from the irradiation in ambient air. In addition, the photo-induced surface flattening was also investigated using the reflection-mode OM in a quantitative manner, which supported the SEM observations and supplied deep insight into the process as well. The experiments and calculation indicate that the photoinduced deformation occurring in the upper parts of IAC-4 microspheres can be decomposed into the mass transfer parallel to the substrate (the x axis) and that towards the substrate (the $-z$ axis). Increasing the refractive index n_{me} (from 1 to 1.491) enhances the shape elongation parallel to the x-axis and reduces the deformation in the $-z$ direction, which lead to the different morphologies of the deformed particles. In consequence, under the same irradiation conditions, the particles subjected to the irradiation in the aqueous media exhibit the larger elongation parallel to the substrate plane, and possess the more flattened upper surfaces, compared with those obtained in air-ambient condition. The aqueous media change the light refraction behavior and the direction of the electric vibration of the polarized light in the microspheres and deformed particles as well. Increasing n_{me} of the medium increases E_{2x}^2 and reduces E_{2z}^2 of the electric field, which correspondingly affects the mass transfer direction. On the other hand, the viscosity η_{me} of the aqueous media (in a range from 0.797 to 791.5 mPa s) shows no detectable effect on the mass transfer behavior, and other factors related to the use of different types of the immersion media also show no effect on the process. Another noticeable change caused by using the aqueous immersion media is that the photo-thermal effect on the mass transfer behavior is ruled out as the thermal dissipation through a liquid is much more efficient than that through air. The method to induce mass transfer with irradiation in aqueous immersion media is not limited to the ten-micron-sized microspheres, where its applicability is also demonstrated by using the submicron periodic structures of IAC-4. This work not only supplies deep understanding of the mass transfer behavior in various immersion media, but also develops a new methodology for the shape manipulation of nano/micro-structures in the aqueous media under light irradiation.

Author contributions

Hao Huang: conceptualization, methodology, investigation, formal analysis, visualization, writing – original draft. Zenan Wang and Xu Li: investigation, resources. Fan Yang: formal analysis, validation. Yechao Su: investigation. Jianhong Xu: validation, resources. Xiaogong Wang: project administration, supervision, writing – review & editing.

Conflicts of interest

There are no conflicts of interest to declare.

Acknowledgements

Notes and references

1 A. Natansohn and P. Rochon, *Chem. Rev.*, 2002, **102**, 4139–4176.
2 S. Lee, H. S. Kang and J. Park, *Adv. Mater.*, 2012, **24**, 2069–2103.
3 J. Plain, G. P. Wiederrecht, S. K. Gray, P. Royer and R. Bachelot, *J. Phys. Chem. Lett.*, 2013, **4**, 2124–2132.
4 A. Priimagi and A. Shevchenko, *J. Polym. Sci., Part B: Polym. Phys.*, 2014, **52**, 163–182.
5 X. G. Wang, *Azo Polymers: Synthesis, Functions and Applications*, Springer, Berlin, 2017.
6 S. L. Oscurato, M. Salvatore, P. Maddalena and A. Ambrosio, *Nanophotonics*, 2018, **7**, 1387–1422.
7 V. Y. Chang, C. Fedele, A. Priimagi, A. Shishido and C. J. Barrett, *Adv. Opt. Mater.*, 2019, **7**, 1900091.
8 B. W. Yang, M. M. Yu and H. F. Yu, *ChemPlusChem*, 2020, **85**, 2166–2176.
9 D. Dattler, G. Fuks, J. Heiser, E. Moulin, A. Perrot, X. Y. Yao and N. Giuseppone, *Chem. Rev.*, 2019, **120**, 310–433.
10 P. Rochon, E. Batalla and A. Natansohn, *Appl. Phys. Lett.*, 1995, **66**, 136–138.
11 D. Y. Kim, S. K. Tripathy, L. Li and J. Kumar, *Appl. Phys. Lett.*, 1995, **66**, 1166–1168.
12 S. Bian, J. M. Williams, D. Y. Kim, L. Li, S. Balasubramanian, J. Kumar and S. Tripathy, *J. Appl. Phys.*, 1999, **86**, 4498–4508.
13 D. Neher, U. Pietsch, M. Giersig, L. Brehmer, B. Stiller, P. Karageorgiev and B. Schulz, *Nat. Mater.*, 2005, **4**, 699–703.
14 C. Hubert, A. Rumyantseva, G. Lerondel, J. Grand, S. Kostcheev, L. Billot, A. Vial, R. Bachelot, P. Royer, S. Chang, S. K. Gray, G. P. Wiederrecht and G. C. Schatz, *Nano Lett.*, 2005, **5**, 615–619.
15 Y. B. Li, Y. N. He, X. L. Tong and X. G. Wang, *J. Am. Chem. Soc.*, 2005, **127**, 2402–2403.
16 C. Hsu, Z. D. Xu and X. G. Wang, *Adv. Funct. Mater.*, 2018, **28**, 1802506.

17 C. J. Barrett, A. L. Natansohn and P. L. Rochon, *J. Phys. Chem.*, 1996, **100**, 8836–8842.

18 J. Kumar, L. Li, X. L. Jiang, D. Kim, T. S. Lee and S. Tripathy, *Appl. Phys. Lett.*, 1998, **72**, 2096–2098.

19 M. Saphiannikova and D. Neher, *J. Phys. Chem. B*, 2005, **109**, 19428–19436.

20 M. L. Juan, J. Plain, R. Bachelot, P. Royer, S. K. Gray and G. P. Wiederrecht, *ACS Nano*, 2009, **3**, 1573–1579.

21 A. Ambrosio, P. Maddalena and L. Marrucci, *Phys. Rev. Lett.*, 2013, **110**, 146102.

22 N. S. Yadavalli, F. Linde, A. Kopyshev and S. Santer, *ACS Appl. Mater. Interfaces*, 2013, **5**, 7743–7747.

23 G. Di Florio, E. Bründermann, N. S. Yadavalli, S. Santer and M. Havenith, *Soft Matter*, 2014, **10**, 1544–1554.

24 J. Vapaavuori, A. Laventure, C. G. Bazuin, O. Lebel and C. Pellerin, *J. Am. Chem. Soc.*, 2015, **137**, 13510–13517.

25 M. Böckmann and N. L. Doltsinis, *J. Chem. Phys.*, 2016, **145**, 154701.

26 V. Toshchevikov, J. Ilnytskyi and M. Saphiannikova, *J. Phys. Chem. Lett.*, 2017, **8**, 1094–1098.

27 J. M. Ilnytskyi, V. Toshchevikov and M. Saphiannikova, *Soft Matter*, 2019, **15**, 9894–9908.

28 H. F. Yu, K. Okano, A. Shishido, T. Ikeda, K. Kamata, M. Komura and T. Iyoda, *Adv. Mater.*, 2005, **17**, 2184–2188.

29 Y. Morikawa, T. Kondo, S. Nagano and T. Seki, *Chem. Mater.*, 2007, **19**, 1540–1542.

30 A. E. Schedl, P. T. Probst, C. Meichner, C. Neuber, L. Kador, A. Fery and H. Schmidt, *Soft Matter*, 2019, **15**, 3872–3878.

31 M. Haggui, M. Dridi, J. Plain, S. Marguet, H. Perez, G. C. Schatz, G. P. Wiederrecht, S. K. Gray and R. Bachelot, *ACS Nano*, 2012, **6**, 1299–1307.

32 T. König, V. V. Tsukruk and S. Santer, *ACS Appl. Mater. Interfaces*, 2013, **5**, 6009–6016.

33 T. Ikawa, F. Hoshino, T. Matsuyama, H. Takahashi and O. Watanabe, *Langmuir*, 2006, **22**, 2747–2753.

34 C. Rianna, A. Calabuig, M. Ventre, S. Cavalli, V. Pagliarulo, S. Grilli, P. Ferraro and P. A. Netti, *ACS Appl. Mater. Interfaces*, 2015, **7**, 16984–16991.

35 L. Rossano, C. Cimmino, S. Cavalli, M. Ventre and P. A. Netti, *Adv. Mater. Interfaces*, 2018, **5**, 1800890.

36 A. Puliafito, S. Ricciardi, F. Pirani, V. Čermochová, L. Boarino, N. De Leo, L. Primo and E. Descrovi, *Adv. Sci.*, 2019, **6**, 1801826.

37 Y. B. Li, Y. N. He, X. L. Tong and X. G. Wang, *Langmuir*, 2006, **22**, 2288–2291.

38 Y. Q. Zhou, B. Y. Liu and X. G. Wang, *Polymer*, 2017, **111**, 229–238.

39 H. Huang, Y. C. Su, J. H. Xu and X. G. Wang, *Langmuir*, 2019, **35**, 15295–15305.

40 H. Huang, Y. C. Su, X. R. Zhou, C. Y. Liao, C. Hsu, Y. Du, J. H. Xu and X. G. Wang, *Soft Matter*, 2018, **14**, 5847–5855.

41 J. P. Liu, Y. N. He and X. G. Wang, *Langmuir*, 2009, **25**, 5974–5979.

42 J. Y. Li, L. Z. Chen, J. P. Xu, K. Wang, X. F. Wang, X. H. He, H. Dong, S. L. Lin and J. T. Zhu, *Langmuir*, 2015, **31**, 13094–13100.

43 Y. J. Jeong, K. J. Park, K. Kim, S. Lee and P. J. Yoo, *Polymer*, 2018, **138**, 180–187.

44 H. Huang, C. Zhang, J. X. Lan, Z. N. Wang and X. G. Wang, *Soft Matter*, 2020, **16**, 9746–9757.

45 A. Ryabchun and A. Bobrovsky, *Adv. Opt. Mater.*, 2019, **7**, 1901486.

46 H. Nakano, T. Takahashi, T. Kadota and Y. Shirota, *Adv. Mater.*, 2002, **14**, 1157–1160.

47 M. Kim, E. Seo, D. Vak and D. Kim, *Chem. Mater.*, 2003, **15**, 4021–4027.

48 M. C. Guo, Z. D. Xu and X. G. Wang, *Langmuir*, 2008, **24**, 2740–2745.

49 R. Ichikawa and H. Nakano, *RSC Adv.*, 2016, **6**, 36761–36765.

50 S. Loebner, N. Lomadze, A. Kopyshev, M. Koch, O. Guskova, M. Saphiannikova and S. Santer, *J. Phys. Chem. B*, 2018, **122**, 2001–2009.

51 D. P. Sanders, *Chem. Rev.*, 2010, **110**, 321–360.

52 D. Xia, Z. Ku, S. C. Lee and S. R. J. Brueck, *Adv. Mater.*, 2011, **23**, 147–179.

53 V. Kozlovskaya, B. Xue and E. Kharlampieva, *Macromolecules*, 2016, **49**, 8373–8386.

54 P. J. Scott, C. R. Kasprzak, K. D. Feller, V. Meenakshisundaram, C. B. Williams and T. E. Long, *Polym. Chem.*, 2020, **11**, 3498–3524.

55 R. Budwig, *Exp. Fluids*, 1994, **17**, 350–355.

56 M. Born and E. Wolf, *Principles of Optics: Electromagnetic Theory of Propagation, Interference and Diffraction of Light*, Pergamon, Oxford, 6th edn, 1980.

57 S. J. Yeo, K. J. Park, K. Guo, P. J. Yoo and S. Lee, *Adv. Mater.*, 2016, **28**, 5268–5275.

58 D. Gray, *American Institute of Physics handbook*, McGraw-Hill, New York, 3rd edn, 1972.